Molecular Imaging of Slip in Entangled DNA Solution

Pouyan E. Boukany,[1,2] Orin Hemminger,[1,3] Shi-Qing Wang,[2,*,†] and L. J. Lee[1,3,*,‡]

[1]*Nanoscale Science and Engineering Center for Affordable Nanoengineering of Polymeric Biomedical Devices, The Ohio State University, Columbus, Ohio 43210, USA*

[2]*Department of Polymer Science, University of Akron, Akron, Ohio 44325, USA*

[3]*Department of Chemical and Bimolecular Engineering, The Ohio State University, Columbus, Ohio 43212, USA*

(Received 9 April 2010; published 9 July 2010)

This work obtains the first molecular imaging of wall slip in entangled solutions. Using a combination of confocal fluorescence microscopy and rheometry, molecular images were captured in the nonlinear response regime of entangled DNA solutions. Conformations of DNA molecules were imaged during shear to correlate with the magnitude of wall slip. Interfacial chain disentanglement results in wall slip beyond the stress overshoot. Sufficient disentanglement can produce tumbling of individual DNA in the entangled solutions.

DOI: 10.1103/PhysRevLett.105.027802 PACS numbers: 61.25.he, 83.10.Mj, 83.50.Rp, 83.80.Rs

In all standard simple-shear rheometric measurements, the fluid of interest is sandwiched between two solid surfaces, and no-slip boundary condition is usually specified [1]. The violation of this condition has been reported for many complex fluids including entangled polymers [2–6], wormlike micelles [7–11], colloids [12], emulsions [13], and even for simple fluids at nanoscale [14]. Slip phenomena in polymer solutions or melts have a rich history and are one of the well-studied subjects in soft condensed matter systems due to their practical relevance in industry. However, the molecular origin of slip [15,16] still lacks direct experimental verification.

Several velocimetry techniques have been used, such as nuclear magnetic resonance imaging [7], fringe pattern fluorescence recovery after photobleaching [4], dynamic light scattering [8], ultrasonic speckle velocimetry [9], microparticle image velocimetry [17], and particle tracking velocimetry [18], to measure velocity profiles during simple shear. None of these measurements could directly probe the molecular mechanism for wall slip, due to the limited spatial and temporal resolutions.

In this Letter, we proposed to use entangled aqueous DNA solutions as a model to determine the molecular origin of wall slip by examining conformations and velocities of individual DNA molecules in shear [19,20]. We integrated a commercial rheometer with a confocal fluorescent microscope (CFM) to directly image the conformational changes of stained DNA molecules and carry out simultaneous time-resolved velocimetric and rheometric measurements [Fig. 1(a)]. The schematic representation of rheo-confocal measurement is shown in Fig. 1(b). A custom microscope stage was designed so that the rheometer can fit over the stage mounted onto the confocal microscope with three adjustable screws to ensure alignment. The CCD camera (connected to the CFM with a 100× objective lens) has a field of view about 67 μm × 67 μm. The lateral resolution, axial resolution, and optical slice thickness is 0.18, 0.47, and 0.82 μm, respectively, in our experiments [21]. More details of the confocal system can be found elsewhere [22].

We used highly purified calf thymus DNA from USB Corp. with a weight-average molecular weight M_w of 50×10^6 g/mol or 7.5×10^4 base pairs (bp) and coil size of 0.7 μm [23]. The DNA solutions were made by dissolving

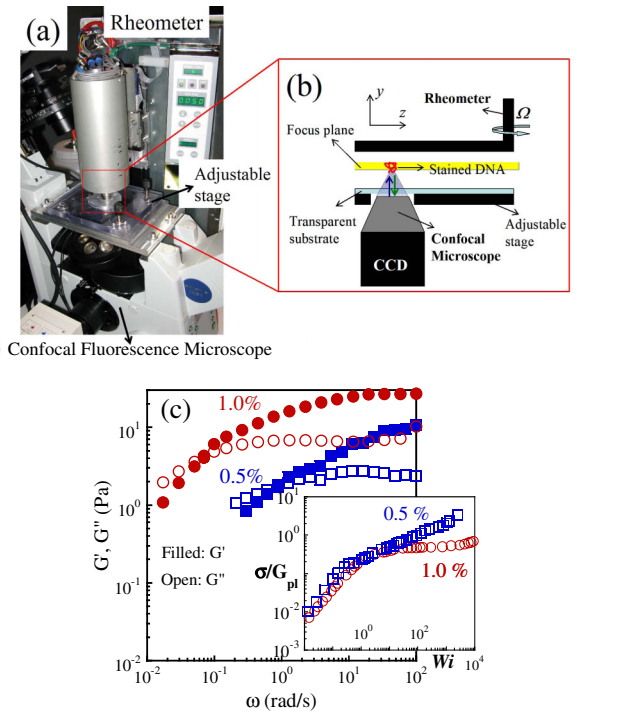

FIG. 1 (color online). (a) Rheometer with the transparent adjustable stage on the Olympus IX-81 inverted fluorescent confocal microscope. (b) Schematic depiction of our rheometric molecular imaging setup. (c) Storage and loss moduli (G' and G'') curves for the two DNA solutions at 23 °C as well as the normalized shear stress σ by the plateau modulus G_{pl} as a function normalized shear rate (i.e., Wi) shown in the inset, where G_{pl} were estimated from the G' and G'' curves.

the DNA in a Tris-EDTA buffer (10 mM tris-HCl +2 mM EDTA +1% NaCl, pH = 8). Care was taken to make homogenous and uniform entangled solutions of DNA in buffer. In order to visualize single molecule dynamics, a tiny amount (0.01 wt % of total DNA added) of fluorescently labeled "probe" DNA molecules was added to the solutions. Yoyo-1 fluorescent dye (Invitrogen Corp.) was used to stain DNA with 1 dye per 5 bp. Uniform molecular mixing of both solutions is confirmed by direct visualization of the prepared sample under CFM [24].

All shear experiments were carried out in controlled-rate mode in a Bohlin CVOR rheometer at room temperature ($T \sim 23\,^{\circ}$C) in either cone-plate (diameter $d = 25$ mm, cone angle $\theta = 2^{\circ}$), or parallel disk ($d = 25$ mm) setup. The bottom plate was a glass cover slip (Fischer Scientific Inc., size 45 × 50 mm, thickness 0.15–0.17 mm, and local roughness <2 nm from atomic force microscopy) placed on the microscope stage, along with a solvent trap to minimize water evaporation during measurements. In this work, the glass cover slips were treated with 3-aminopropyltriethoxysilane to provide strong interaction between DNA and the treated glass surface [25].

First, small amplitude oscillatory shear with strain amplitude $\gamma = 5\%$ was employed to characterize basic linear viscoelastic properties of the DNA solutions as shown in Fig. 1(c). The longest relaxation times τ for the 1.0 and 0.5 wt % DNA solutions were determined to be 14 and 1.1 s, respectively, from the inverse of the crossover frequency where $G' = G''$. With concentration increase from 0.5 to 1.0 wt %, the level of elastic modulus $G_{\rm pl}$ increases, as does the number $Z = M_w/M_e$ of entanglements per chain [26], rising from $Z = 22$ to 55. The inset of Fig. 1(c) shows the steady-state shear stress σ normalized by $G_{\rm pl}$ at different apparent shear rates $\dot{\gamma}_{\rm app}$ as a function of the Weissenberg number (Wi $= \dot{\gamma}_{\rm app}\tau$) for both solutions in cone-plate geometry ($d = 25$ mm, $\theta = 2^{\circ}$). When Wi < 1.0, the normalized stress $\sigma/G_{\rm pl}$ increased linearly with Wi. In the nonlinear regime (Wi > 1.0), the slope of the flow curve changes abruptly, and a wide stress plateau is present in the 1.0 wt % solution.

Simultaneous conformational, velocimetric, and rheometric measurements were then carried out on both entangled solutions of concentrations 0.5 and 1.0 wt %, respectively. These samples were sheared between two parallel disks, with diameter of 25 mm and a gap H of about 60 μm. The point of visualization was 3–4 mm from meniscus of the sample in all measurements. At low shear rates with Wi < 1.0, the stress growth is monotonic [cf. inset of Fig. 2(a)]. The velocity profile was made by tracking the displacement of the stained DNA as a function of time across the sample thickness. As we expected, the velocity profile is linear across the gap at all time [Fig. 2(a)]. DNA chains remained coiled and unperturbed in this Newtonian flow regime [shown in Fig. 2(b)].

When Wi > 1.0, the shear stress overshoot occurred during start-up shear, as shown in Fig. 2(c). The stress

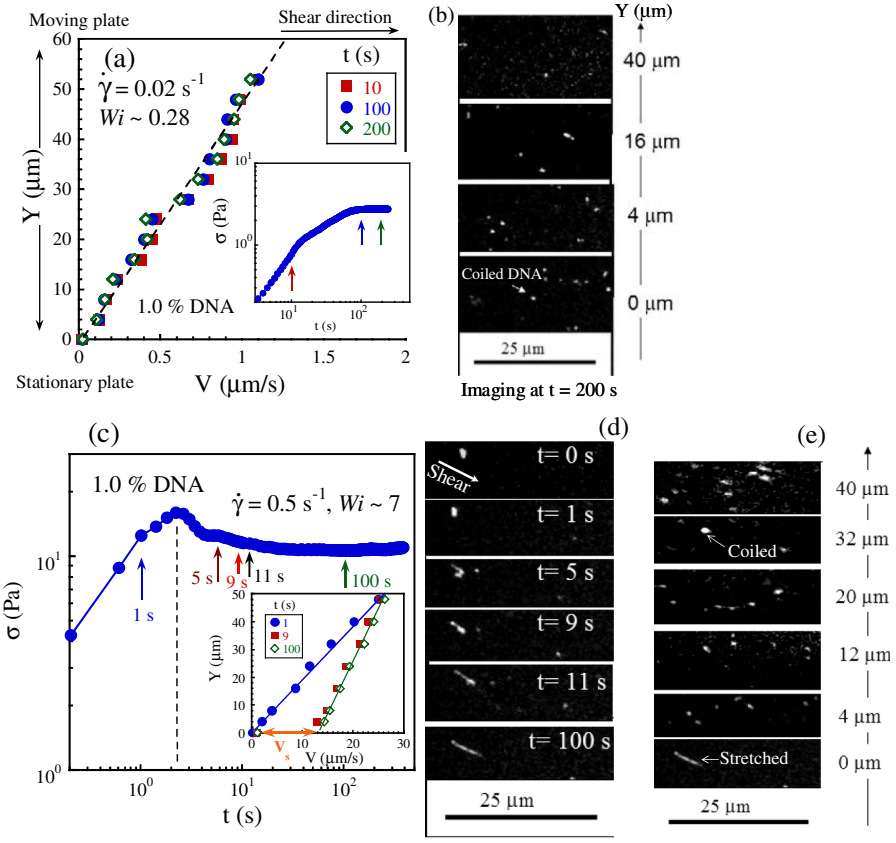

FIG. 2 (color online). (a) Velocity profile in the parallel disk geometry at the shear rate of 0.02 s^{-1} showing homogeneous shear, where the inset shows the shear stress growth as a function of time. (b) Corresponding coiled conformation of DNA anywhere across the gap at this low shear rate. (c) The stress growth as a function of time at $\dot{\gamma}_{\rm app} = 0.5$ s^{-1}, where the inset indicates no slip prior to the stress overshoot and slip afterward the stress maximum. (d) Time-dependent conformational changes of DNA in the slip layer, where the arrow with "Shear" indicates that the DNA orientation is along the shearing direction. (e) The conformation of DNA across the gap during steady slip at $\dot{\gamma}_{\rm app} = 0.5$ s^{-1} (t = 100 s).

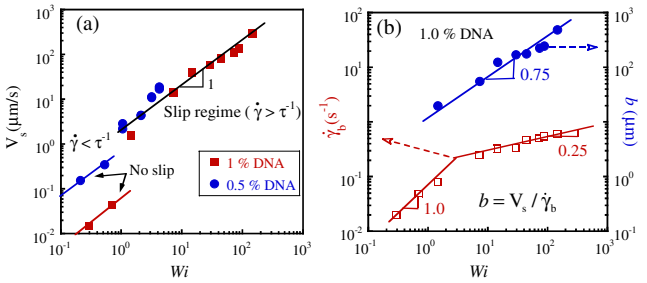

FIG. 3 (color online). (a) Slip velocity V_s versus Wi for both concentrations of 1.0% and 0.5% with $Z = 55$ and 22, respectively. The velocity of bulk DNA molecules close to surface in absence of slip, i.e., for $\mathrm{Wi} < 1$, obeys $V_{\mathrm{ns}} = R_g \times \dot{\gamma}_{\mathrm{ns}}$, where R_g is the coil size and $\dot{\gamma}_{\mathrm{ns}}$ is the imposed shear rate. (b) The scaling of the bulk shear rate $\dot{\gamma}_b$ and slip length b as a function of Wi for 1.0% DNA.

grows from zero and increases monotonically, indicating elastic deformation under no-slip boundary condition, as shown in the inset. By focusing on the bottom stationary wall, we not only monitor the speed of the tracked DNA molecules at the interface but also capture their conformational changes. Initially, the adsorbed DNA was coiled. Beyond the stress overshoot, the adsorbed DNA became disentangled with bulk DNA chains since the nonbounded DNA at the interface picked up speed at this moment ($t \sim 5$ s). Figure 2(d) shows that the absorbed chain also started to get elongated. The DNA remained stretched in the shearing direction. Slip is rather significant at $t = 9$ s, as shown in the inset of Fig. 2(e). At steady state ($t = 100$ s and beyond), the magnitude of wall slip reaches a steady value. Figure 2(e) shows the DNA conformations at the different positions along the sample thickness. Molecules were disentangled only in the first monolayer where adsorbed chains were stretched, and the molecules everywhere else remained coiled and essentially entangled, as evidenced by the small bulk shear rate.

With increasing applied Wi, the amount of wall slip grows. Capturing the molecular imaging under shear at different rates, we have evaluated how the slip velocity V_s within one monolayer at the interface and the bulk shear rate $\dot{\gamma}_b$ change with Wi. Based on information similar to that presented in Fig. 2(c), we found in Fig. 3(a) that slip occurs only for $\mathrm{Wi} > 1$ and V_s grows essentially linearly with Wi. The data are consistent with the expected simple relationship between the velocity V of the displacing surface and slip velocity V_s: $V = \alpha V_s + \dot{\gamma}_b H$, where α is a number between 1 and 2, depending on whether slip occurs on only the bottom surface or on both the top and the bottom surface. Formally [15], $V_s = \sigma/\beta$, where β is given by viscosity η_i in the slip layer divided by the layer thickness a, and its maximum $V_{s(\mathrm{max})} = \sigma a/\eta_s$ involves the solvent viscosity η_s. Since $V/H = \dot{\gamma}_{\mathrm{app}}$, we have $\mathrm{Wi} = \alpha(V_s/H)\tau + \dot{\gamma}_b\tau$, where $\dot{\gamma}_b\tau$ is on the order of unity as long as $\dot{\gamma}_{\mathrm{app}} < V_{s(\mathrm{max})}/H$.

The video-imaging scan over the sample thickness reveals that the bulk shear rate $\dot{\gamma}_b \sim \mathrm{Wi}^{0.25}$. Conversely, the slip length $b = V_s/\dot{\gamma}_b \sim \mathrm{Wi}/\mathrm{Wi}^{0.25} \sim \mathrm{Wi}^{0.75}$, as shown in Fig. 3(b). It is worth noting that the increase of b with Wi is not boundless, and the different levels of wall slip correspond to different amounts of chain disentanglement between adsorbed and bulk chains.

At $\mathrm{Wi} = 70$ and beyond the stress overshoot, we not only observed significant wall slip but saw evidence for full chain disentanglement. For example, apart from the considerable slip indicated by the high speed of the DNA molecules just next to the solid surface, as shown in Fig. 4(a), we observed oscillatory conformational change in these molecules. These DNA molecules in the slip layer stayed stretched most of the time. They also spent a small fraction of the time to tumble as shown in Fig. 4(b). This

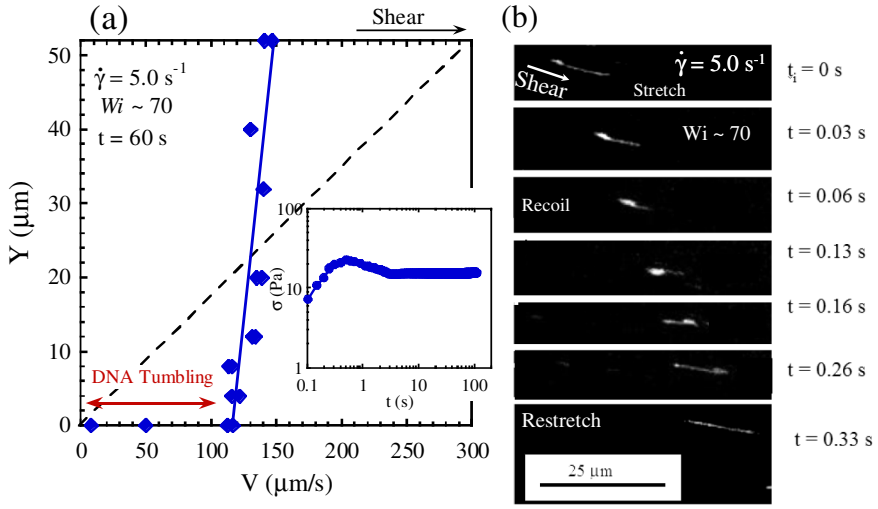

FIG. 4 (color online). (a) Steady-state velocity profile at $\dot{\gamma}_{\mathrm{app}} = 5.0\ \mathrm{s}^{-1}$ and $t = 60$ s, with the inset showing the shear stress growth. (b) The corresponding conformations of DNA in the slip layer during tumbling in steady state (at $t = 60$ s) at an apparent shear rate of $5.0\ \mathrm{s}^{-1}$.

remarkable tumbling behavior indicates that the DNA molecules in the slip layer are free from surface adsorption and fully disengaged from the entanglement network. In contrast, no tumbling was detected at lower Wi, suggesting that the DNA molecules were only partially disentangled. Specifically, the tumbling of the DNA molecule takes less than 0.05 s, indicating a local shear rate faster than 20 s^{-1} while spending a long time (about 1 s) to remain stretched and nontumbling. DNA tumbling has previously been observed only in dilute nonentangled solutions [27]. The observed tumbling in entangled solutions confirms that a disentanglement state is one of free chains not so different from those in dilute solutions.

In closing, we mention that when interactions between a substrate [e.g., a poly(methyl methacrylate) surface] and DNA chains are weak, massive wall slip takes place without any observable stretching of DNA molecules at the surface. Here, lack of chain entanglement due to chain desorption produces wall slip and assures coiled conformations for all DNA [28]. This desorption-induced wall slip makes sharp contrast with the cohesive wall slip discussed above, where the molecular imaging has provided the first molecular evidence for the chain disentanglement mechanism for wall slip of entangled polymers. Since the rheological characteristics of such DNA solutions are identical to those of neutral synthetic polymer solutions, and enough salt is present to make the DNA neutralized, the present evidence should be sufficiently useful and serve the purpose to offer a physical picture for wall slip of all well entangled polymeric liquids sheared by strongly adsorbing surfaces.

We would like to acknowledge Malvern Instrument for lending us a Bohlin-CVOR rheometer and Edward Laughlin and Sham Ravindranath at the University of Akron for design and fabrication of the adjustable and mountable stage for the confocal fluorescent microscope. This work is, in part, supported by the National Science Foundation under NSF Grants No. EEC-0425626 and No. DMR-0821697.

*Corresponding author.
†swang@uakron.edu
‡Lee.31@osu.edu

[1] R. G. Larson, *The Structure and Rheology of Complex Fluids* (Oxford University Press, New York, 1999).
[2] M. Denn, Annu. Rev. Fluid Mech. **33**, 265 (2001), and references therein.
[3] S. G. Hatzikiriakos and J. M. Dealy, J. Rheol. **35**, 497 (1991); F. Koran and J. M. Dealy, J. Rheol. **43**, 1291 (1999).
[4] K. B. Migler, H. Hervet, and L. Leger, Phys. Rev. Lett. **70**, 287(1993); G. Massey, H. Hervet, and L. Leger, Europhys. Lett. **43**, 83 (1998); L. Leger, Adv. Polym. Sci. **138**, 185 (1999); L. Leger, J. Phys. Condens. Matter **15**, S19 (2003).
[5] P. Drda and S. Q. Wang, Phys. Rev. Lett. **75**, 2698 (1995); for a review see S. Q. Wang Adv. Polym. Sci. **198**, 673 (1999); P. E. Boukany, P. Tapadia, and S. Q. Wang, J. Rheol. **50**, 641 (2006).
[6] L. A. Archer, R. G. Larson, and Y. L. Chen, J. Fluid Mech. **301**, 133 (1995); V. Mhetar and L. A. Archer, Macromolecules **31**, 6639 (1998); T. T. Dao and L. A. Archer, Langmuir **18**, 2616 (2002).
[7] P. T. Callaghan *et al.*, J. Phys. II (France) **6**, 375 (1996); R. Mair and P. T. Callaghan, Europhys. Lett. **36**, 719 (1996).
[8] J. B. Salmon *et al.*, Phys. Rev. Lett. **90**, 228303 (2003).
[9] L. Becu, S. Manneville, and A. Colin, Phys. Rev. Lett. **93**, 018301 (2004); J. P. Decruppe *et al.*, Phys. Rev. E **73**, 061509 (2006); S. Manneville *et al.*, Phys. Rev. E **75**, 061502 (2007); M. Paul Lettinga and S. Manneville, Phys. Rev. Lett. **103**, 248302 (2009).
[10] A. Mendez-Sanchez, J. Rheol. **47**, 1455 (2003).
[11] P. E. Boukany and S. Q. Wang, Macromolecules **41**, 1455 (2008).
[12] I. Cohen *et al.*, Phys. Rev. Lett. **97**, 215502 (2006).
[13] L. Beuc, S. Manneville, and A. Colin, Phys. Rev. Lett. **96**, 138302 (2006).
[14] O. I. Vinogradova *et al.*, Phys. Rev. Lett. **102**, 118302 (2009); S. Granick, Y. Zhu, and H. Lee, Nature Mater. **2**, 221 (2003); Y. Zhu and S. Granick, Phys. Rev. Lett. **87**, 096105 (2001); **88**, 106102 (2002); J. L. Barrat and L. Bocquet, Phys. Rev. Lett. **82**, 4671 (1999).
[15] F. Brochard and P. G. de Gennes, Langmuir **8**, 3033 (1992); F. Brochard-Wyart, C. Gay, and P. G. deGennes, Macromolecules **29**, 377 (1996).
[16] P. E. Boukany and S. Q. Wang, Macromolecules **42**, 2222 (2009).
[17] Y. T. Hu and A. Lips, J. Rheol. 49, 1001 (2005).
[18] S. Q. Wang, Macromol. Mater. Eng. **292**, 15 (2007).
[19] P. LeDuc, C. Haber, G. Bao, and D. Wirtz, Nature (London) **399**, 564 (1999).
[20] D. E. Smith, H. P. Babcock, and S. Chu, Science **283**, 1724 (1999); H. P. Babcock *et al.*, Phys. Rev. Lett. **85**, 2018 (2000); E. S. G. Shaqfeh, J. Non-Newtonian Fluid Mech. **130**, 1 (2005), and references therein.
[21] J. S. Park, C. K. Choi, and K. D. Kihm, Exp. Fluids **37**, 105 (2004).
[22] O. Hemminger *et al.*, in *Proceedings of the 12th International Conference on Fluidization, Vancouver, 2007* (Engineering Conferences International, Brooklyn, NY, 2007), pp. 489–496.
[23] The coil size is evaluated according to $R_g = 2l_p(aN/12lp)^{\nu}$ with $a = 0.34$ nm being the length of base pair, $N = 7.5 \times 10^4$ bp, the persistence length $l_p = 0.050\ \mu$m, $\nu = 0.5$ for θ solvent [T. G. Mason *et al.*, Macromolecules **31**, 3600 (1998)].
[24] R. E. Teixeria *et al.*, Macromolecules **40**, 2461 (2007).
[25] J. Jing *et al.*, Proc. Natl. Acad. Sci. U.S.A. **95**, 8046 (1998).
[26] The critical entanglement molecular weight $M_e(C)$ can be estimated from the plateau modulus $G_{\rm pl}$ evaluated from Fig. 1(c): $M(C) = CRT/G_{\rm pl}(C)$, where C, R, and T are the concentration, gas constant, and temperature, respectively.
[27] R. E. Teixeria *et al.*, Macromolecules **38**, 581 (2005).
[28] P. E. Boukany, O. Hemminger, S. Q. Wang, L. J. Lee (unpublished).